(Received 25 July 2025, Accepted 4 February 2026, Scheduled 24 March 2026)

Design of a Tunable Wide-Stopband Plasmonic Filter Based on a Metal-Insulator-Metal (MIM) Waveguide for Mid-Infrared Applications

Ahmed Lounis[1, *], Imane Zegaar[2], Hocine Bensalah[3], and Abdesselam Hocini[1]

[1] *Laboratoire d'Analyse des Signaux et Systèmes, Department of Electronics University of M'Sila BP.166, Route Ichebilia, M'Sila 28000, Algeria*
[2] *LIST Laboratory, University of M'Hamed Bougara Boumerdes Avenue of Independence, Boumerdes 35000, Algeria*
[3] *Université Yahia Fares Médéa, Algeria*

ABSTRACT: Wide-stopband plasmonic filters are critical components for the development of compact mid-infrared (MIR) photonic systems. In this study, we propose a geometrically tunable wide-stopband plasmonic filter based on a meta-insulator-metal (MIM) waveguide integrated with dual resonator cavities. The optical response of the proposed structure is numerically investigated using the two-dimensional finite-difference time-domain (2D-FDTD) method. We systematically analyze the influence of key geometric parameters, specifically the resonator height ($H2$) and inter-cavity distance (D), on the stopband characteristics. Our results demonstrate that the symmetric dual-cavity configuration provides effective control over both the stopband bandwidth and central wavelength. Consequently, the proposed design achieves a significantly broadened stopband while preserving structural compactness and high transmission selectivity, making it a highly promising candidate for integration into advanced MIR photonic circuits and sensing systems.

1. INTRODUCTION

Electromagnetic surface waves, known as surface plasmon polaritons (SPPs), propagate along the interface between a metal and a dielectric material. These waves result from the strong coupling between the electromagnetic field and the collective oscillations of free electrons at a metal surface. Due to their unique ability to confine and guide light at subwavelength scales, SPPs have emerged as one of the most promising candidates for the realization of plasmonic integrated circuits (PICs). Unlike conventional dielectric waveguides, SPP-based structures can overcome the diffraction limit, enabling light manipulation and transmission in nanoscale optical devices with enhanced integration density [1].

Among various plasmonic waveguide configurations, the metal-insulator-metal (MIM) waveguide stands out for its high confinement of optical energy within the dielectric layer and relatively straightforward fabrication process. This architecture enables strong field localization and offers an excellent platform for developing miniaturized photonic components. MIM waveguides serve as a versatile foundation for constructing a wide range of on-chip plasmonic devices, including waveguide filters, couplers, and sensors [2]. Numerous device designs based on MIM waveguides have been proposed and studied extensively, such as plasmonic filters for spectral shaping and filtering applications [3, 4], high-sensitivity sensors for biochemical detection [5, 6], and efficient optical couplers for routing and signal transfer within integrated circuits [7, 8].

In recent years, plasmonic waveguide structures based on metal-insulator-metal (MIM) configurations have attracted considerable attention due to their strong field confinement and potential for compact integration in mid-infrared (MIR) photonic systems. The fundamental behavior of surface plasmon polaritons (SPPs) at metal-dielectric interfaces has been thoroughly described in classical studies [9–11], providing the theoretical foundation for modern plasmonic devices. The modal dispersion and coupling mechanisms of MIM waveguides have been extensively investigated to optimize mode propagation and minimize loss [12–14]. The reliable modeling of optical constants is also essential, with the Johnson and Christy data [15] and subsequent updates [16–18] remaining the standard reference for noble metals in the MIR range.

Building upon these advances, several studies have proposed tunable and multi-band plasmonic filters designed for on-chip mid-infrared applications, demonstrating remarkable control over resonance characteristics and transmission bandwidth [19–23]. Despite these achievements, most existing designs still face trade-offs among bandwidth selectivity, fabrication complexity, and insertion losses. Therefore, the development of a compact and tunable wide-stopband plasmonic filter remains an open research challenge with significant potential for MIR photonic integration, an issue directly addressed in the present work.

Recently, there has been growing interest in developing band-stop filter (BSF) devices based on SPPs due to their pivotal role in optical communication systems, signal processing,

* Corresponding author: Ahmed Lounis (ahmed.lounis@univ-msila.dz).

and spectrum selection technologies [24]. These devices are essential for suppressing unwanted frequency components and enhancing signal integrity in photonic networks.

In the present work, we propose and analyze a novel stopband optical filter that leverages the SPP propagation in an MIM waveguide structure coupled with resonator cavities.

The design is numerically investigated using RSoft CAD software in combination with the two-dimensional finite-difference time-domain (2D FDTD) simulation technique to accurately capture the electromagnetic behavior and spectral response of the device.

The 2D FDTD model represents an effective-index approximation of the planar MIM structure, which has been shown to reliably capture resonance trends and stopband formation in similar geometries.

The filter exhibits a distinct stopband characteristic within the mid-infrared range. Importantly, the performance and spectral position of the stopband can be effectively tuned by adjusting the structural parameters of the cavity resonators, offering flexibility in meeting specific optical system requirements. This tunability and compact footprint make the proposed filter highly suitable for integration in next-generation plasmonic circuits and optical communication modules.

2. STRUCTURE DESIGN AND ANALYSIS METHOD

Our proposed device is shown in Figure 1. It is composed of a waveguide connected to a resonator cavity. The filter parameters $L1$, $L2$, $L3$, and W are fixed at 200 nm, 300 nm, 150 nm, and 50 nm, respectively. This filter's metal area is silver (Ag), and its dielectric region is air. The optical response of silver was modeled using a single-pole Drude model [25]:

$$\varepsilon_m = \varepsilon_\infty - \frac{\omega_p^2}{\omega^2 - i\omega\gamma} \tag{1}$$

with parameters $\varepsilon_\infty = 3.7$, $\omega_p = 1.38 \times 10^{16}$ rad/s, $\gamma = 2.73 \times 10^{13}$ rad/s) fitted to the tabulated optical constants of Palik [10]. This model provides accurate results within the investigated mid-infrared spectral range. To verify reliability, the results were compared with those obtained from a multi-oscillator model [11, 12], showing consistent spectral behavior while preserving computational efficiency.

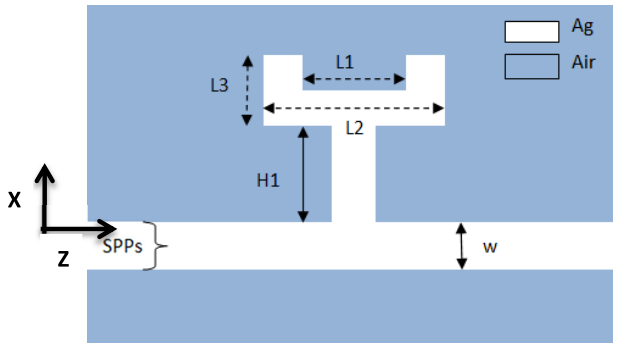

FIGURE 1. Schematic diagram of proposed filter.

Because of its high electrical conductivity and superior optical performance in the visible and near-infrared spectrums, silver (Ag) is generally considered one of the best materials for surface plasmon waveguides. It effectively facilitates surface plasmon polariton (SPP) propagation, allowing high-frequency optical signals to be transmitted with little loss. Because of its tremendous absorption and low dispersion, silver is a very useful material for creating sophisticated optical components. Its surfaces also offer localized surface plasmon enhancement, which greatly increases the optical sensitivity of molecules or compounds in close proximity to one another. This is a crucial characteristic for optical sensing, detection, and amplification applications.

A thin layer of silver (Ag) is placed on a silica substrate (SiO_2). Next, an E-beam photoresist layer performs a spin coating. A bespoke shape is then created on the photoresist layer by exposing this layer to an E-beam lithography. The Ag layer can be selectively removed by chemical etching and development. Ultimately, the residual layer of photoresist is eliminated [26].

The transmission characteristics of the proposed plasmonic filter structure are investigated through detailed numerical simulations using RSoft CAD software in conjunction with the Finite-Difference Time-Domain (FDTD) method. This approach allows for the accurate modeling of complex electromagnetic interactions within the structure, particularly in the presence of subwavelength features. To ensure that outgoing electromagnetic waves do not reflect back into the computational domain and distort the simulation results, Perfectly Matched Layer (PML) boundary conditions are employed. These PMLs act as artificial absorbing layers surrounding the simulation area, effectively mimicking an open and infinite space by absorbing all incident waves, regardless of their angle or frequency.

The mesh size was carefully chosen below 10 nm to accurately resolve the strong field confinement within the 50 nm dielectric core and the skin depth in silver at mid-infrared wavelengths. The Courant stability factor was set to 0.5, and convergence tests were conducted by refining the spatial grid and verifying that the transmission spectra remained unchanged within 1%. The source was a broadband TM-polarized plane wave covering the 2–10 μm range, and field monitors were placed along the propagation direction to record the transmission and reflection spectra.

To reduce computational complexity while maintaining high accuracy, two-dimensional (2D) simulations are performed. Although three-dimensional simulations offer a more complete physical picture, the 2D approximation provides substantial computational savings in terms of time and memory requirements. This is especially practical in plasmonic systems, where the third dimension does not significantly influence the propagation characteristics for certain geometries. Previous studies have shown that 2D FDTD simulations can deliver highly reliable results for planar plasmonic waveguide structures, making them an efficient tool for initial device design and optimization [27].

In the case of metal-insulator-metal (MIM) waveguides, only the fundamental transverse magnetic (TM_0) mode can be effi-

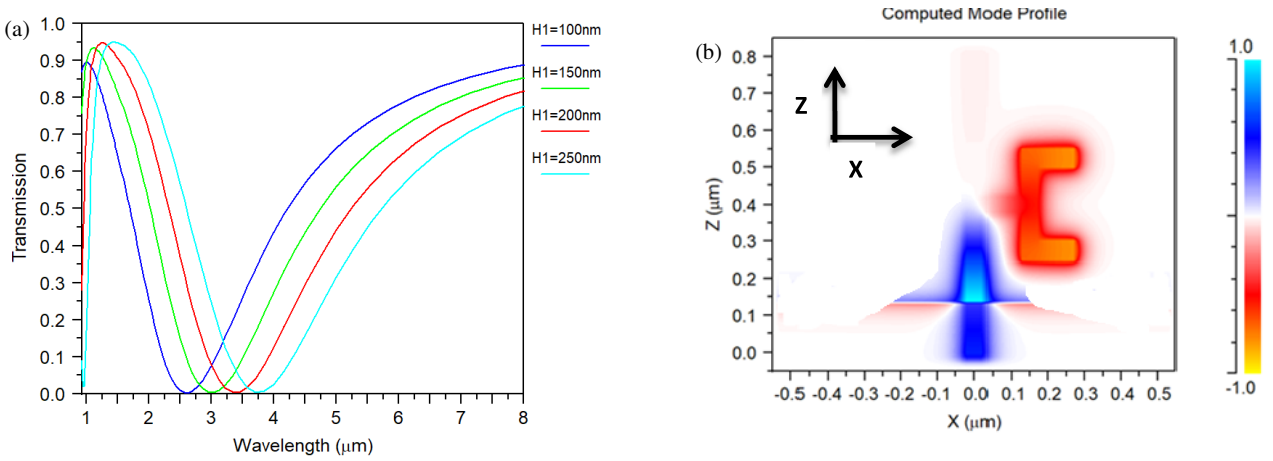

FIGURE 2. (a) Response spectrum of the designed filter for various $H1$. (b) The proposed structure's magnetic field distribution at the resonance wavelengths.

ciently excited and supported due to the narrow width of the waveguide relative to the operating wavelength. This mode is characterized by having the electric field component perpendicular to the direction of propagation (i.e., in the vertical direction across the insulator layer), and it exhibits strong confinement within the dielectric core. Higher-order modes are cut off under these dimensions and operating conditions, making TM_0 the dominant mode of interest in the analysis.

The resonant behavior of the cavity integrated into the MIM waveguide can be accurately described in terms of the TM_0 mode. The resonance wavelength depends on several factors, including the effective refractive index, cavity length, and boundary conditions imposed by surrounding metal interfaces. The resonance condition can be approximately modeled using analytical or semi-analytical expressions derived from waveguide theory, enabling us to predict the spectral location of the stopband. Such cavity-enhanced filtering mechanisms are critical in designing compact, high-performance plasmonic devices for integrated optical systems [28].

$$\lambda_m = \frac{2R_e\left(n_{eff}\right) l_{eff}}{m}, \quad m = 1, 2, 3 \tag{2}$$

where $R_e(n_{eff})$ signifies the real part of the SPP's effective refractive index, and l_{eff} is the resonator's effective resonance length.

The transmission spectrum of the optical filter with various values of $H1$ (100 to 250) nm is illustrated in Figure 2(a). A clear redshift of the resonance wavelength is observed as $H1$ increases, which results from the elongation of the optical path and stronger confinement within the side-coupled cavity. The stopband gradually shifts from 2.6 μm for $H1 = 100$ to approximately 3.8 μm for $H1 = 250$ nm, demonstrating the tunability of the filter through simple geometric modification.

The band gap width was quantitatively defined as the full width, where the transmission drops 0.1 below the maximum transmission in the passband. The maximum transmission in the passband provides a clear criterion for evaluating the stopband performance. This definition is now used consistently throughout the manuscript to quantitatively describe the stopband region.

Among the analyzed cases, $H1 = 100$ nm provides the most favorable spectral characteristics, including the deepest stopband (minimum transmission $\approx$ 0.1) and a broad, flat passband beyond 3.5 μm. This combination corresponds to an optimal trade-off between coupling strength and radiative losses. The results confirm that the resonance originates from destructive interference between the main waveguide and side-coupled cavity modes, and that tuning $H1$ effectively controls the spectral position of this interference.

Furthermore, the magnetic field distribution at the resonance wavelength of 2.6 μm is illustrated in Figure 2(b). As shown in the figure, the incident electromagnetic energy becomes strongly localized within the resonator cavity, indicating effective coupling between the waveguide mode and the cavity. This strong field confinement is a hallmark of resonance behavior in plasmonic structures and is crucial for achieving high-performance filtering in subwavelength devices.

To further enhance the filter's performance, a second resonator — identical in geometry and dimensions to the first —

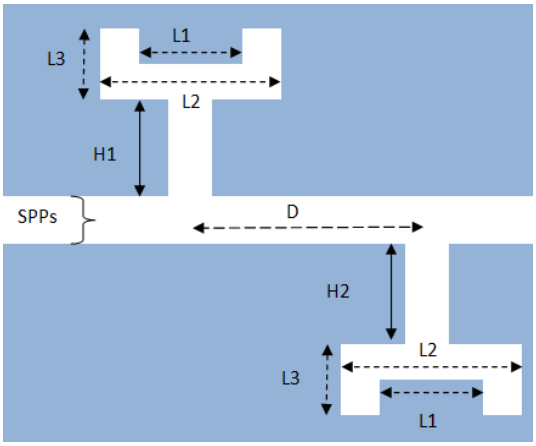

FIGURE 3. 2D schematic illustration of proposed device with double cavities.

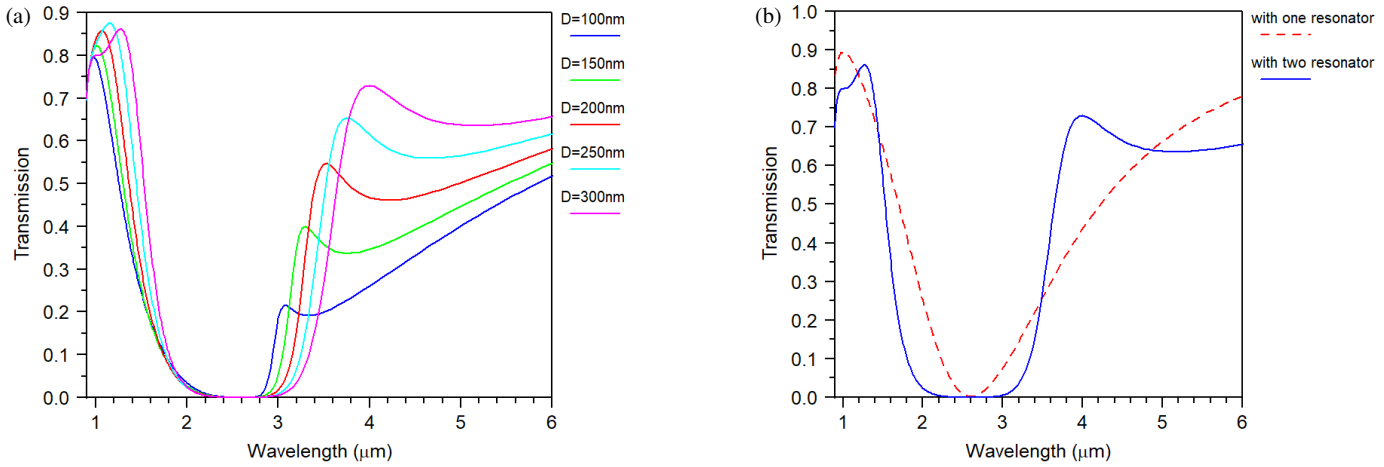

FIGURE 4. (a) Response spectrum of a stopband filter with double cavities for various D. (b) Response spectrum of a filter with one and two cavities at $D = 300$ nm.

is symmetrically added to the opposite side of the MIM waveguide, as illustrated in Figure 3. This dual-resonator configuration is designed to increase the interaction length between the propagating surface plasmon polaritons (SPPs) and the resonant cavities, thereby offering a more pronounced stopband and improved control over the transmission spectrum.

The influence of the inter-cavity distance (D) between the two resonators is systematically investigated, with simulation results presented in Figure 4(a). As the separation distance D increases from 100 nm to 300 nm, notable changes in the transmission spectrum are observed. Specifically, the passband transmittance on the lower-wavelength side of the stopband improves significantly, and the overall transmission profile evolves into a distinct U-shaped curve. This spectral shaping effect is attributed to constructive and destructive interference between the fields coupled through the two resonators, which becomes more optimized at specific separation distances.

The U-shaped transmission profile arises from the interference between the resonances of the two symmetrically placed cavities, which modifies the effective coupling strength and redistributes spectral suppression across the stopband.

Additionally, Figure 4(b) compares the transmission spectra of two filter configurations: one with a single resonator (represented by the dashed line) and the other with two resonators (represented by the solid line). It is evident that the band-gap width in the dual-resonator configuration is considerably broader (0.96 μm) than that in the single-resonator case, indicating enhanced filtering capabilities. This broadening is a result of increased cavity coupling and mode interference introduced by the second resonator.

As a result of this parametric study, it is concluded that the optimal inter-resonator distance for achieving maximum bandwidth and improved spectral shaping is 300 nm. This configuration balances coupling strength and resonance alignment, making it a favorable design for efficient and compact plasmonic stop-band filters.

For the next study, of our analysis, we focused on evaluating the impact of varying the height ($H2$) of the second resonator cavity on the overall performance of the proposed plasmonic stopband filter. This investigation is critical, as geometric parameters, such as cavity height, play a significant role in tuning the resonant behavior and spectral characteristics of the filter.

The transmission spectra corresponding to different values of $H2$ are presented in Figure 5(a). As can be observed, increasing $H2$ from 50 nm to 200 nm leads to a noticeable redshift in the center wavelength of the stopband. This shift toward longer wavelengths is attributed to the increase in the effective optical path length within the resonator, which in turn alters the resonance condition for the supported surface plasmon polariton (SPP) modes.

Additionally, Figure 5(b) demonstrates that not only does the central resonance wavelength shift, but the bandwidth of the filtered wavelength range also increases. Specifically, as $H2$ increases, the stopband becomes significantly broader within the mid-infrared (MIR) region, enhancing the device's capability to block a wider range of unwanted frequencies. This tunable broadening effect is advantageous for applications that require flexible spectral control and dynamic filtering over a broad wavelength span.

To quantitatively assess the impact of $H2$ on the filter's spectral behavior, the filtered wavelength bands corresponding to each tested $H2$ value are summarized in Table 1. These tabulated data provide a clear comparison and support the conclusion that $H2$ can be effectively utilized as a tuning parameter to precisely control both the location and width of the stopband.

These findings confirm the high tunability of the proposed MIM-based plasmonic filter, making it a suitable candidate for

TABLE 1. The filtered wavelength band with different values of $H2$.

$H2$ (nm)	Filtered Wavelengths Band
50	$\lambda_1 = 1.90\,\mu$m, $\lambda_2 = 2.88\,\mu$m
100	$\lambda_1 = 2.10\,\mu$m, $\lambda_2 = 3.06\,\mu$m
150	$\lambda_1 = 2.25\,\mu$m, $\lambda_2 = 3.3\,\mu$m
200	$\lambda_1 = 2.34\,\mu$m, $\lambda_2 = 3.57\,\mu$m

TABLE 2. Comparison of our proposed device with different band-stop plasmonic filters.

Reference	The range of the filtered wavelengths	The band gap width	Resonator forma
[29]	$[\lambda_1 = 850.0\,\text{nm}, \lambda_2 = 1300\,\text{nm}]$	450 nm	T-shaped
[30]	$[\lambda_1 = 1350\,\text{nm}, \lambda_2 = 1900\,\text{nm}]$	550 nm	Teeth-shaped
[31]	$[\lambda_1 = 1180\,\text{nm}, \lambda_2 = 1950\,\text{nm}]$	770 nm	Stub-shaped
This study	$[\lambda_1 = 2340\,\text{nm}, \lambda_2 = 3570\,\text{nm}]$	1230 nm	Stub connected with U-shaped

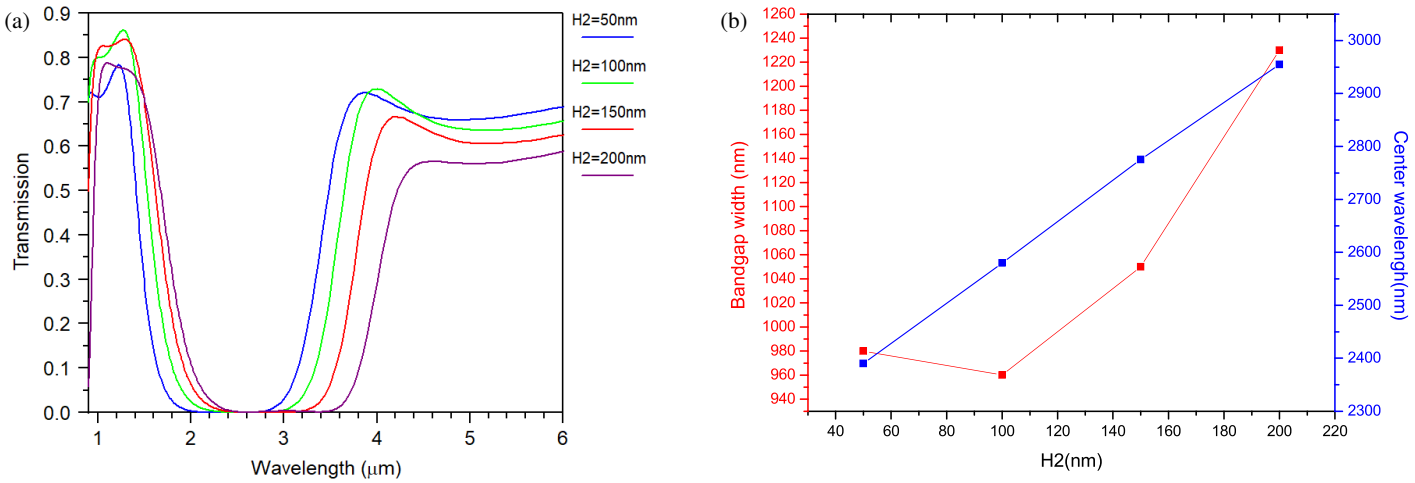

FIGURE 5. (a) Response spectra of the proposed device for various $H2$. (b) Band gap width and center wavelength of the filter with various $H2$.

adaptive photonic systems in sensing, communication, and signal processing applications across the MIR spectrum.

Table 2 presents a comparative analysis between the proposed wide-stopband plasmonic filter and previously reported MIM-based designs in terms of stopband range and bandwidth. All the structures listed are based on metal-insulator-metal (MIM) waveguides coupled with resonator cavities of various geometries. The results clearly indicate that the proposed configuration achieves a broader stopband coverage than prior works, demonstrating its superior filtering performance and design efficiency.

3. CONCLUSION

In this work, a tunable wide-stopband plasmonic filter based on a metal-insulator-metal (MIM) waveguide coupled with dual resonator cavities was designed and analyzed for mid-infrared applications. Numerical simulations using the 2D finite-difference time-domain (FDTD) method demonstrated that introducing a symmetric second resonator significantly enhances the stopband performance by increasing both its width and spectral tunability. The separation distance D between the resonators governs the spectral shape, where increasing D leads to the emergence of a U-shaped transmission profile due to enhanced coupling effects.

Moreover, varying the height of the secondary resonator $H2$ enables precise control over the central wavelength and stopband width, allowing for a customizable spectral response. The tuning of the stopband characteristics is achieved through geometrical parameter adjustment ($H2$ and D) during the design stage. Owing to its compact configuration, high design flexibility, and efficient spectral control, the proposed structure is a promising candidate for mid-infrared photonic integrated circuits, optical sensing, and selective wavelength suppression in communication systems.

REFERENCES

[1] Zavvari, M., M. T. H. Azar, and A. Arashmehr, "Tunable band-stop plasmonic filter based on square ring resonators in a metal-insulator-metal structure," *Journal of Modern Optics*, Vol. 64, No. 20, 2221–2227, 2017.

[2] Zegaar, I., A. Hocini, and H. Ben Salah, "Modeling and analysis of the RI sensitivity of plasmonic sensor based on MIM waveguide-coupled structure," *Journal of Physics: Conference Series*, Vol. 1859, No. 1, 012024, 2021.

[3] Khatooni, H. S., K. Abbasian, and T. Nurmohammadi, "A tunable band-stop plasmonic waveguide filter and switch designing with triangular resonator based on Kerr non-linearity," *Optik*, Vol. 224, 165708, 2020.

[4] Zegaar, I., A. Hocini, A. Harhouz, D. Khedrouche, and H. Salah, "Design of a double-mode plasmonic wavelength filter using a defective circular nano-disk resonator coupled to two MIM waveguides," *Progress In Electromagnetics Research Letters*, Vol. 104, 67–75, 2022.

[5] Ghorbani, S., M. Sadeghi, and Z. Adelpour, "Investigation and analysis of a tunable plasmonic filter based on the Kerr nonlinear effect of a gold nanocomposite," *Laser Physics*, Vol. 30, No. 8, 086201, 2020.

[6] Harhouz, A. and A. Hocini, "Highly sensitive plasmonic temperature sensor based on Fano resonances in MIM waveguide coupled with defective oval resonator," *Optical and Quantum Electronics*, Vol. 53, No. 8, 439, 2021.
[7] Zaki, A. O., K. Kirah, and M. A. Swillam, "Hybrid plasmonic electro-optical modulator," *Applied Physics A*, Vol. 122, No. 4, 473, 2016.
[8] Das, S., A. Salandrino, J. Z. Wu, and R. Hui, "Near-infrared electro-optic modulator based on plasmonic graphene," *Optics Letters*, Vol. 40, No. 7, 1516–1519, 2015.
[9] Maier, S. A., *Plasmonics: Fundamentals and Applications*, Springer, 2007.
[10] Dmitriev, V. A. and A. O. Silva, "Nonreciprocal properties of surface plasmon-polaritons at the interface between two magnetized media: Exact analytical solutions," *Progress In Electromagnetics Research Letters*, Vol. 21, 177–186, 2011.
[11] Ozbay, E., "Plasmonics: Merging photonics and electronics at nanoscale dimensions," *Science*, Vol. 311, No. 5758, 189–193, 2006.
[12] Kuttge, M., E. J. R. Vesseur, J. Verhoeven, H. J. Lezec, H. A. Atwater, and A. Polman, "Loss mechanisms of surface plasmon polaritons on gold probed by cathodoluminescence imaging spectroscopy," *Applied Physics Letters*, Vol. 93, No. 11, 113110, 2008.
[13] Halterman, K., J. M. Elson, and P. L. Overfelt, "Characteristics of bound modes in coupled dielectric waveguides containing negative index media," *Optics Express*, Vol. 11, No. 6, 521–529, 2003.
[14] Butt, M. A., "Review of innovative cavity designs in metal-insulator-metal waveguide-based plasmonic sensor," *Plasmonics*, Vol. 20, 4257–4276, 2025.
[15] Johnson, P. B. and R. W. Christy, "Optical constants of the noble metals," *Physical Review B*, Vol. 6, No. 12, 4370, 1972.
[16] McMahon, J. M., S. K. Gray, and G. C. Schatz, "Nonlocal optical response of metal nanostructures with arbitrary shape," *Physical Review Letters*, Vol. 103, No. 9, 097403, 2009.
[17] Law, S., D. C. Adams, A. M. Taylor, and D. Wasserman, "Mid-infrared designer metals," *Optics Express*, Vol. 20, No. 11, 12 155–12 165, 2012.
[18] Derkachova, A., K. Kolwas, and I. Demchenko, "Dielectric function for gold in plasmonics applications: Size dependence of plasmon resonance frequencies and damping rates for nanospheres," *Plasmonics*, Vol. 11, No. 3, 941–951, 2016.
[19] Wang, H., J. Yang, J. Zhang, J. Huang, W. Wu, D. Chen, and G. Xiao, "Tunable band-stop plasmonic waveguide filter with symmetrical multiple-teeth-shaped structure," *Optics Letters*, Vol. 41, No. 6, 1233–1236, 2016.
[20] Lu, H., X. Liu, D. Mao, L. Wang, and Y. Gong, "Tunable band-pass plasmonic waveguide filters with nanodisk resonators," *Optics Express*, Vol. 18, No. 17, 17 922–17 927, 2010.
[21] Zhou, Z., L. Liu, X. Li, J. Shen, G. Han, and Z. Li, "Dual-band bandpass plasmonic filter based on effective localized surface plasmon resonators," *Applied Computational Electromagnetics Society Journal (ACES)*, Vol. 37, No. 10, 1031–1038, Oct. 2022.
[22] Anusha, P., K. Srihari, and S. Karthik, "Reconfigurable plasmonic waveguides based on phase-change materials for on-chip optical switching," *Plasmonics*, Vol. 21, No. 1, 1415–1424, 2026.
[23] Huang, S., H. Wang, and S. Shen, "Multiband tunable perfect absorber based on graphene metamaterials," *Physica Scripta*, Vol. 100, 045519, 2025.
[24] Zegaar, I., A. Hocini, D. Khedrouche, H. B. salah, and H. bahri, "Plasmonic stop-band filter based on an MIM waveguide coupled with cavity resonators," *Journal of Physics: Conference Series*, Vol. 2240, No. 1, 012025, 2022.
[25] Salah, H. B., H. Bahri, A. Hocini, I. Zegaar, S. Ingebrandt, and V. Pachauri, "Design of a plasmonic sensor based on a nano-sized structure for biochemical application," *Journal of Physics: Conference Series*, Vol. 2240, No. 1, 012024, 2022.
[26] Kazanskiy, N. L., M. A. Butt, and S. N. Khonina, "Nanodots decorated MIM semi-ring resonator cavity for biochemical sensing applications," *Photonics and Nanostructures — Fundamentals and Applications*, Vol. 42, 100836, 2020.
[27] Salah, H. B., A. Hocini, M. N. Temmar, and D. Khedrouche, "Design of mid infrared high sensitive metal-insulator-metal plasmonic sensor," *Chinese Journal of Physics*, Vol. 61, 86–97, 2019.
[28] Hocini, A., H. B. Salah, D. Khedrouche, and N. Melouki, "A high-sensitive sensor and band-stop filter based on intersected double ring resonators in metal-insulator-metal structure," *Optical and Quantum Electronics*, Vol. 52, No. 7, 336, 2020.
[29] Pooretemad, S., A. Malekijavan, and M. Aslinezhad, "Ultrawideband bandstop filter based on Fano resonance and rectangular resonators," *Applied Optics*, Vol. 60, No. 14, 4266–4272, 2021.
[30] Zhai, X., L. Wang, L.-L. Wang, X.-F. Li, W.-Q. Huang, S.-C. Wen, and D.-Y. Fan, "Tuning bandgap of a double-tooth-shaped MIM waveguide filter by control widths of the teeth," *Journal of Optics*, Vol. 15, No. 5, 055008, 2013.
[31] Zegaar, I., A. Hocini, H. Bensalah, A. Harhouz, D. Khedrouche, and M. Lahoubi, "Ultra wideband bandstop plasmonic filter in the NIR region based on stub resonators," *Physica Scripta*, Vol. 98, No. 5, 055510, 2023.